The modelling of growing natural forms, part II

Huw Jones and Jaap Kaandorp

Lansdown centre for Electronic Arts, Middlesex University, London, UK
Faculty of Mathematics, Computer Science, Physics & Astronomy
University of Amsterdam, Amsterdam, The Netherlands

3. Modelling growth and form of sponges and stony corals

This section will be structured in three parts: "Growth in abiotic processes and bacteria" (Section 3.1), "Growth in marine sessile organisms" (Section 3.3) and "Diffusive patterning mechanisms" (Section 3.7). In the first part we will discuss some (relatively) simple growth processes found in for example physical deposition processes and in growth of bacteria colonies. In Section 3.2 it will be demonstrated how these growth patterns can be modelled using partial differential equations and probabilistic cellular automata. In the second part on the sponges and stony corals, we will use these results to construct more evolved models (discussed in Sections 3.4 - 3.6), which can be applied to model growth and form of marine sessile organisms and the influence of the physical environment (the dispersion of food particles through hydrodynamics). In the third part models will be discussed which can be used to simulate the biological (genetical) regulation of the growth processes and why sponges and stony corals are an attractive case study for this.

3.1. Growth in abiotic processes and bacteria

Many growth processes in nature are not in equilibrium. An extreme example is an aggregation process of particles where as soon as a particle is added to the growth form, it stops trying other sites an no further rearrangement takes place. The local probabilities that the object grows are not everywhere equal on the aggregate and an instable situation emerges. The growth process in non-equilibrium is relatively fast and often irregular objects, characterised by a fractal dimension, are formed [10], [32], [31]. An example of a growth process, in non-equilibrium from physics, is viscous fingering [9]. The phenomenon can be demonstrated in a experiment where air displaces a high-viscosity fluid between two glass plates. In fig. 1 a diagram is shown of an experiment where air is injected between two glass plates at $y = 0$ and displaces a high viscosity fluid, which is only removed at the top of the plates (both sides are closed). The pressure P will be the highest at $y = 0$ and the lowest at $y = L$, where L represents the length of the glass plates. In the fluid the pressure is given by the Laplace equation:

$$-\nabla^2 P = 0 \tag{1}$$

In the air the pressure is everywhere equal, since its viscosity can be ignored. The pressure in the air equals to the input pressure P(y=0) and the consequence is that the largest pressure gradients occur at the tips of the fingers in fig. 1, while the lowest gradients occur below the tips. The probability that the fingers continue to grow will be the highest at the tips and in a next growth stage the pressure gradients in the tips are still more amplified, resulting in an instable situation. In fig. 2 an example of the resulting growth pattern is shown, it is an irregular shaped object, known in the literature as viscous fingering.

Another example of growth in non-equilibrium is growth of a bacteria colony (for example *Bacillus subtilis*) on a petri-dish [10] [2] [1]. The colony consumes nutrients from its immediate environment and the distribution of nutrients is determined by diffusion. When it is assumed that the concentration c is zero at the colony and that the diffusion process is fast compared to the growth process, the concentration field will attain a steady state in which the diffusion equation

$$\frac{dc}{dt} = \mathcal{D}_{diffusion} \nabla^2 c \tag{2}$$

equals zero. In this equation $\mathcal{D}_{diffusion}$ is the diffusion coefficient. The nutrient source may be, for example, a circle around the colony or a linear source where the concentration is maximal. The local nutrient concentration at sites between the colony and the source can be described with the Laplace equation:

$$\nabla^2 c = 0 \tag{3}$$

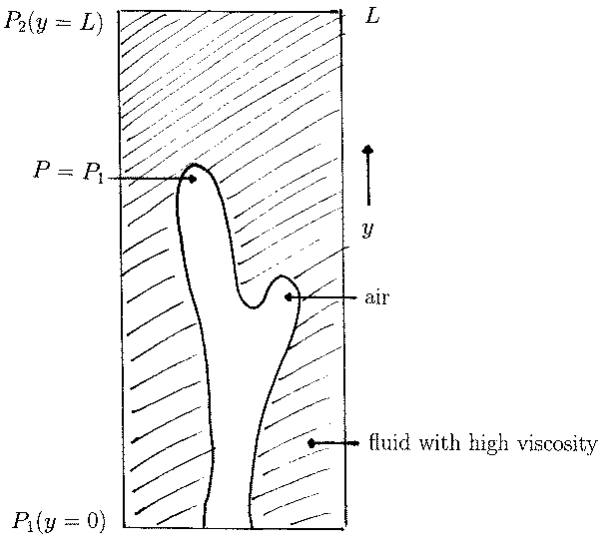

Figure 1: Diagram of a viscous fingering experiment

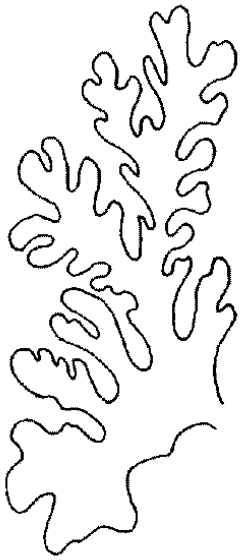

Figure 2: Example of a viscous fingering growth pattern

3.2. Modelling Diffusion limited aggregation using cellular automata

The growth process of a bacteria colony, viscous fingering, and various other growth patterns from physics as for example electric discharge patterns and growth forms of electro deposits, can be simulated with one model: the Diffusion Limited Aggregation model [31]. At the heart of all these growth patterns there is one Partial Differential Equation, the Laplace equation, which describes the distribution of the concentration (Eq. 3), pressure (Eq. 1), electric potential etc. in the environment of the growth pattern. The DLA-model is a probabilistic cellular automaton which resides on a square two-dimensional or three dimensional lattice. The growth pattern can be constructed using the following Monte Carlo approach. The first step in the construction is to occupy a lattice site with a seed. After that, particles are released from a circle (using the seed as a centre) or from line at a large distance from the seed. The particle starts a random walk, the walk stops when the particles leaves the circle or reaches a perimeter site of the seed and sticks. Then more random walkers are released from the source and are allowed to walk until the distance with respect to the cluster with occupied sites becomes too large or it reaches a perimeter site, neighbouring to one of the previous particles, and it sticks. In fig. 3 the first stages are shown of the formation of the growth pattern. When this procedure is repeated many times an irregular growth pattern as shown in fig. 4 is generated. The cluster depicted in fig. 4 was generated on a 1000 x 1000 lattice, using a linear source at the top and a seed positioned at the bottom of the lattice. The fractal dimension D_{box} of this growth form can be determined by applying the box-counting method [9]. In this case the D_{box} is about 1.7. The underlying Laplace equation in this Monte Carlo approach is solved by mimicking a diffusion process using random moving particles.

To obtain more insight in the nutrient distribution around the DLA-cluster the underlying Laplace equation can be solved numerically and a DLA cluster can, alternatively, be constructed using the nutrient distribution over the lattice. The cluster is initialised with a seed and the following boundary conditions are applied: $c = 0$ on the cluster itself and $c = 1$ at the nutrient source, which may be circular, linear etc. The cluster is constructed using the following rules in the probabilistic cellular automaton:

```
1    solve the Laplace equation (Eq. 3),
     using the boundary conditions c = 0
     on the cluster
     and c = 1 at the nutrient source
2    new sites are added to the cluster
     with probability p (Eq. 4)
3    goto 1
```

The probability p that a perimeter site (the sites indicated with an open circle in fig. 3 with index k will be added to the

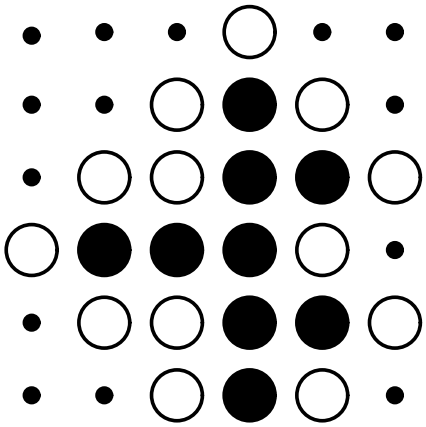

Figure 3: First steps in the construction of the DLA-cluster. Sites which are part of the cluster are visualised as black circles, sites which are possible candidates to be added to the cluster in next iteration steps are indicated with open circles.

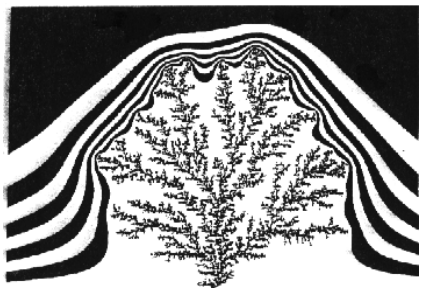

Figure 4: DLA-cluster generated on a 1000 x 1000 lattice using a linear source of nutrient, located at the top row of the lattice .

DLA-cluster (black circles in fig. 3) is determined by

$$p(k \in \circ \rightarrow k \in \bullet) = \frac{(c_k)^\eta}{\sum_{j \in \circ}(c_j)^\eta} \qquad (4)$$

where $c_k =$ concentration at position k

The exponent η applied in eq. 4 describes the relation between the local field and the probability. This exponent usually ranges in experiments from 0.0 to 2.0. The sum in the denominator represents the sum of all local concentrations of the possible growth candidates (the open circles in fig. 3). The Laplace equation can be solved, using the boundary conditions mentioned above, by finite differencing and the successive over-relaxation method (see for example [27]):

$$c_{i,j}^{n+1} = \qquad (5)$$
$$\frac{\omega}{4}(c_{i-1,j}^{n+1} + c_{i,j-1}^{n+1} + c_{i+1,j}^{n} + c_{i,j+1}^{n}) +$$
$$(1-\omega)c_{i,j}^{n}$$

In this method the new local nutrient concentration in the lattice $c_{i,j}^{n+1}$, at a site with lattice co-ordinates i, j , is determined in an iterative procedure which converges as soon as the difference between the new and old local nutrient concentration ($c_{i,j}^{n+1} - c_{i,j}^{n}$) is below a certain tolerance level. The ω in Eq. 5 is the over-relaxation parameter, which in general lies within the range $1 \leq \omega \leq 2$. With this alternative construction of the DLA-cluster it becomes possible to visualise the basins of equal nutrient ranges around the growth pattern in fig. 4. The nutrient concentration decreases when the black or white basin is situated close to the object. The concentration in the white basin that surrounds the growth pattern is almost zero. In the example of fig. 4 a linear source of nutrient is used, positioned at the top row of the lattice and the exponent η in Eq. 4 is set to unity. From fig. 4 it can be observed that the probability that new sites will be added to the cluster will be the highest at the tips of the cluster, where the steepest nutrient gradients occur, and the lowest in the bays between the branches. In successive growth steps the nutrient gradients at the tips will even become steeper and a comparable instable situation is encountered as in the viscous fingering example (figs. 1 and 2).

The effect of changing the exponent η in Eq. 4 is that the overall shape of the cluster changes. For the value $\eta = 0$ the shape changes in a compact cluster and it can be demonstrated that the DLA-model for this special case transforms into the Eden model. This model is one of the earliest probabilistic cellular automata to simulate growth. In the Eden model each possible growth candidate in fig. 3 has the same probability to become occupied. For the value $\eta = 1$ the "normal" DLA-cluster is obtained, while for higher values more dendritic shapes are generated [23]. With the parameter η the effect of nutrient gradients on the growth process can be controlled, where the Eden model is an extreme example in which gradients have no effect on the local probability that a new site will be added to the growth form. The objects which can be generated by varying η in the range 0.0-2.0, can be compared to each other using the box dimension D_{box}. The value of D_{box} in experiments where η is set to the values 0.0, 0.5, 1.0, and 2.0; becomes respectively 2.0, 1.8, 1.7, and 1.5. This decrease in D_{box} in this range indicates a decrease in irregularity or space-filling properties of the perimeters of the objects.

The DLA-model is useful as a simulation model for a wide range of growth patterns from nature. The fractal dimension D_{box} = 1.7 of the DLA-cluster with $\eta = 1$ seems to correspond quite well with the D_{box} of several real growth patterns. It should be noted that D_{box} is only one aspect of the morphology, it is possible to generate objects with a very different overall morphology with equal fractal dimensions. A very interesting property of the DLA-model is that it includes a model of the physical environment on the growth process. Several phenomena that can be observed in experiments with the bacteria *Bacillus subtilus* [10] can be predicted with this model. It can for example be predicted that the shape of the nutrient source (linear, circular etc.) has no

influence on the degree of irregularity, as expressed in the value of D_{box}, of the colony.

3.3. Growth in marine sessile organisms

In marine sessile organisms, as for example sponges, stony-corals, and hydro-corals, two different sources of energy are used. The first energy source is light necessary for the photosynthesis, the second one consists of filter-feeding by capturing suspended material in the immediate environment. In many cases, as for example in many stony-corals [5], hydro-corals, and some sponges [36] a combination of both energy sources is used, while many sponges are exclusively suspension feeders.

In many sponges, stony-corals, and hydro-corals the growth form emerges in an accretive growth process [11] [14] [35], in which layers of new material are added on top of the preceding growth stages of the organisms. In most cases the preceding growth stages remain unchanged. Although this type of growth process is relatively simple compared to for example seed plants and vertebrates, growth forms with a highly complex geometry emerge. The environmental influence on the growth, which consists of light and the availability of suspended material, is relatively simple compared to the environmental influence on the growth process of terrestrial organisms. These two properties make marine sessile organisms an excellent case study for developing models of morphogenesis.

In both types of energy sources, as well in the case of the mixed energy source (partly photosynthetic and partly filter-feeding) there is a strong impact of the physical environment on the growth process, where local light intensities and the local availability of nutrients, determine the local growth velocities and consequently the form. Many marine sessile suspension feeders from various taxonomical groups, as for example sponges, hydrocorals, and stony corals, exhibit a strong morphological plasticity, which is in many cases related to the impact of hydrodynamics. The exposure to water movement represents one of the dominant environmental parameters. There is a strong impact of hydrodynamics on the growth process. In a number of cases it is possible to arrange growth forms of sponges, hydrocorals, and stony corals along a gradient of the amount of water movement [16]. In Veron and Pichon [34] several series of growth forms of stony corals (for example *Pocillopora damicornis*) are shown, which are arranged along a gradient of the amount of water movement. In the examples of both stony corals, the growth form gradually transforms from a compact shape under exposed conditions, to a thin-branching one under sheltered conditions. In Fig. 5 two extreme examples of growth forms are shown of *Pocillopora damicornis*. Form A originates from a site sheltered to water movement, while B was collected from an exposed site. Between both extremes, a range of gradually changing intermediate growth forms exist.

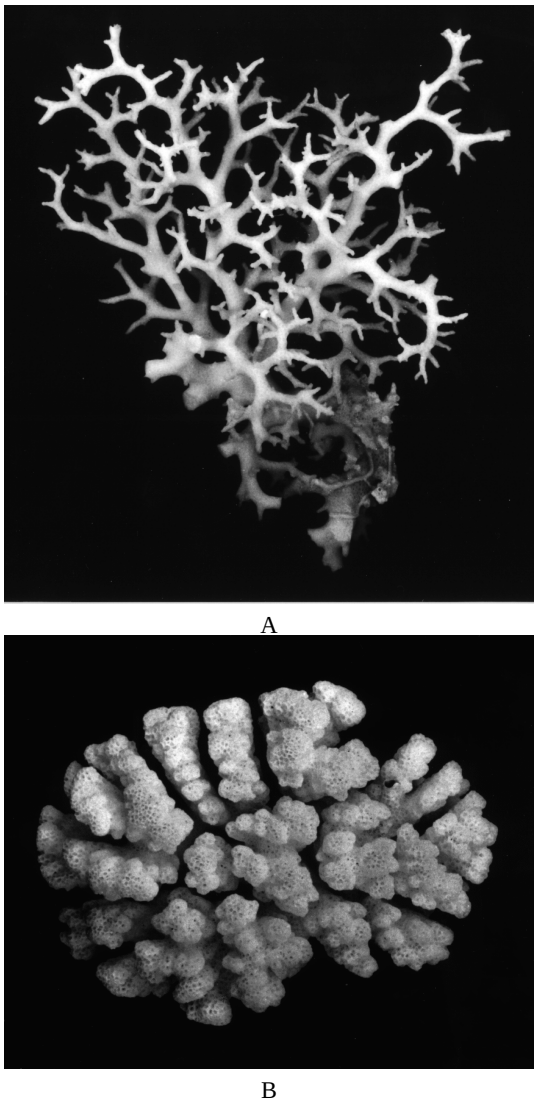

A

B

Figure 5: *Growth forms of the stony coral* Pocillopora damicornis. *Form A originates from a site sheltered to water water movement, form B originates from an exposed site*

In this tutorial we will mainly focus ourselves to the influence of the local available amount of suspended material on the deposition of new material during the growth process. In a model of the morphogenesis of an organism, in which suspension feeding represents a significant part of the energy intake, two compononents are relevant. The first component is a model of the growth process and the second is a model of the influence of the nutrient distribution on the local growth velocities.

In the absence of flow the distribution of nutrients around the growth form can be modelled as a diffusion process in a steady state: there is a source of suspended material and

the organism consumes continuously nutrients from its environment. In general, in a marine environment, there will be a significant contribution of the hydrodynamics to the dispersion pattern of the suspended material around the growth form. In this case the distribution of nutrients around the organism will be determined by a combination of flow and diffusion. The contribution of flow to the nutrient distribution of nutrients can be quantified by the Péclet number:

$$Pe = \frac{\overline{u}l}{D} \tag{6}$$

where $\overline{u}$ is the average flow velocity, l a characteristic length in the system, and D the diffusion coefficient. In the diffusion limited case Pe is very small (nearly zero), while in the flow dominated case Pe is large.

In this tutorial we will discuss a method to model a nutrient distribution determined by a combination of diffusion and flow, and we will show how this nutrient distribution can be included in a model of a growth process. The method which we have applied is the lattice Boltzmann method. We will give a brief introduction to the method in Section 3.4, a more detailed account of this method is given in [6] [20] [21] [18]. Two books providing a good introduction to this method are [7] and [30]. The flow pattern around the growth form is modelled using the lattice Boltzmann method, this method can be combined with a tracer step, in which populations of "particles" move over the nodes of the lattice. In this tracer step the joint effect of flow and diffusion on the nutrient distribution can be studied. This method is especially suitable for modelling diffusion and flow phenomena in biological systems. In this method boundary conditions with a complex geometry can be easily specified. The Péclet number and the Reynolds number can be varied independently [20]. In addition we can take advantage of the fact that the method is very suitable for scalable implementions on Massive Parallel Computers [28], which allows for the required large scale simulations of biological systems.

The time complexity of the simulation problem we are dealing with is such that we have to apply HPC-techniques in order to attain acceptable simulation times. Moreover the memory complexity of the 3D growth models impose a cubic memory requirement. Therefore to simulate systems with a realistic size (lattices with a size above 100^3 are needed in the nutrient distribution computations) the memory requirements exceed by far the amount available on a typical high-end workstation. By exploiting the locality of the lattice Boltzmann solver we can map the simulation to a parallel distributed memory machine and use a large amount of available local memory and at the same time minimize the amount of communication.

We will use two different types of growth processes as case-studies in this tutorial. The first type is the aggregation model in which growth is modelled as the addition of particles and where the growth form is represented in discrete space. This model can be applied to simulate very "basic" growth patterns as for example found in bacteria colonies [10]. The second growth model will be a geometric model for accretive growth, this model will be briefly discussed in Section 3.5.2, more details can be found in [14]. In [19] we discuss how this growth model can be combined with a model of a nutrient distribution caused solely by diffusion, in [19] we demonstrate how the computionally most expensive part of the complete model, solving the diffusion equation with a "classical" method (finite-differencing and Successive Over Relaxation), can be parallized and be combined with a sequential version of the growth model. We have applied a similar hybrid approach for accretive growth: the growth is represented is in continuous space, while the nutrient distribution is approximated in discrete space using the lattice Boltzmann method.

3.4. Modelling the nutrient distribution using the lattice Boltzmann method

In the simulations a cubic lattice is used, where each node is connected with 18 other nodes. There are 6 links with the length of one lattice unit and 12 links with the length of $\sqrt{2}$ units. All parameters and variables in the lattice Boltzmann method are expressed in lattice units. The mean populations of particles travel simultaneously from one node to one of the 18 neighbours. The evolution of the lattice is described by the following dynamical rule:

$$n_i(r + c_i, t + 1) = n_i(r, t) + \Delta_i(r, t) \qquad i = 1, .., 18 \tag{7}$$

where $n_i(r,t)$ is the continuous velocity distribution function, which describes the number of particles of particles at a node at position r, at time t and with direction c_i. The moments of the distribution function $n_i(r,t)$:

$$\rho = \sum_i n_i \tag{8}$$

$$j = \sum_i n_i c_i = \rho u$$

$$\Pi = \sum_i n_i c_i c_i$$

correspond to the hydrodynamic fields mass density ρ, momentum density j (u is the flow group velocity at node r), and momentum flux Π.

A linearized collision operator $\mathcal{L}_{ij}$ about an apropriate equilibrium n^{eq} can be constructed:

$$\Delta_i(n) = \Delta_i(n^{eq}) + \sum_j \mathcal{L}_{ij}(n_j - n_j^{eq}) \tag{9}$$

where $\Delta_i(n^{eq}) = 0$ by definition since the equilibrium is collision invariant, and where n^{eq} is the Maxwell Boltzmann distribution for a gas. The distribution function can be splitted into an equilibrium and a non-equilibrium part:

$$n_i = n_i^{eq} + n_i^{neq} \tag{10}$$

Similar to Eq. 8 the moments of the equilibrium distribution function n_i^{eq} are:

$$\rho = \sum_i n_i^{eq} \tag{11}$$
$$j = \sum_i n_i^{eq} c_i$$
$$\Pi = \sum_i n_i^{eq} c_i c_i = p1 + \rho uu$$

where p is the pressure and 1 is the unit vector. The momentums of the particles are changed by adding an external force, the driving force F, to the system. The particle collisions conserve mass and momentum but change the non-equilibrium part of the momentum flux:

$$\Pi^{neq} = \Pi + \Pi^{eq} \tag{12}$$

By using properties as conservation of mass, momentum, and symmetry, it is possible to construct a number of eigenvalue equations (see for a more detailed account of the collision process [20]) for the moments of $\mathcal{L}_{ij}$:

$$\sum_i \mathcal{L}_{ij} = 0 \tag{13}$$
$$\sum_i c_i \mathcal{L}_{ij} = 0$$
$$\sum_i \overline{c_i c_i} \mathcal{L}_{ij} = \lambda \overline{c_j c_j}$$
$$\cdots$$

where $\overline{c_i c_i}$ indicates the traceless part of $c_i c_i$ ($\overline{c_i c_i} = c_i c_i - \frac{1}{3} c_i^2 1$). The first two equations conserve mass and momentum. The eigenvalue λ is related to the shear viscosity:

$$\nu = -\frac{1}{6}\rho(2/\lambda + 1) \tag{14}$$

One computational update of the lattice now involves a propagation step where n_i particles travel from node r to node $r + c_i$ and a collision step in which the post-collision distribution $n_i + \Delta_i(n)$ is determined in the following three steps. First at each node ρ, j, and Π are calculated and the equilibrium momentum flux Π^{eq} is determined. In the second step the momentum flux, including the equilibrium and nonequilibrium part, can be updated using the moments of the linearized collision operator in Eq. 13. In the third step, after the post collision momentum is computed, the post-collision distribution $n_i + \Delta_i(n)$ can be calculated.

In the simulations two types of boundary conditions are used: at the borders of the lattice periodic boundary conditions are applied, while in the nodes adjacent to the nodes representing the obstacle, solid boundary conditions are used. Periodic boundary conditions can be implemented by exchanging the n_i's of the links at the borders of the lattice. Solid boundary conditions can be represented by exchanging the n_i's between the adjancent node and a neighbouring fluid node.

After the lattice Boltzmann iteration a tracer step is applied where populations of tracer particles are released from well defined source nodes, while the tracer particles are absorbed by the sink nodes: the nodes adjacent to the growth form. The tracer particles can move from a node at site r in the lattice to one of the 18 adjacent nodes $r + c_i$, where the Péclet number determines if flow or diffusion dominates. In the simulations ν is set to the value $\frac{1}{6}$, while the diffusion coefficient D varies, and $\overline{u}$ is kept constant by the adjusting the driving force F of the system. Due to the growth of the aggregate, without adjustment of the driving force, the velocity in the free fluid would gradually decrease.

3.5. Modelling the growth process of marine sessile organisms

3.5.1. Growth by aggregation

In the aggregation process the growth process is modelled in a similar way as done in the Diffusion Limited Aggregation model [37]. In Fig. 6 the basic construction of the aggregate is shown. The cluster is initialized with a "seed" positioned at the bottom plane of the lattice. The bottom plane, "the substrate", is positioned at the xz-plane at $y = 1$, while the seed is one lattice site, located at the position $(xmax/2, 2, zmax/2)$. In both the cluster and substrate sites solid boundary conditions are applied. The flow in the lattice is directed from the yz-plane at $x = 0$ to the yz-plane at $x = xmax$. The flow velocity in the free fluid nodes is kept to a constant value $\overline{u}$. The flow pattern about the obstacle (substrate and cluster) is determined in the lattice Boltzmann iteration, using 10 iteration steps, and followed by a tracer step. In each growth step 10 iteration steps are used to ensure that an equilibrium is obtained in the flow pattern. In the last step tracer particles are released from the source plane, the lattice sites in the xz-plane at $y = ymax$. The tracer particles are absorbed by the nodes adjacent to the sites in the substrate plane (the xz-plane at $y = 1$) and the aggregate. In the sink nodes the amount of absorbed tracer particles is determined and a new node is added to the cluster. The probability p that k, an element from the set of open circles $\circ$ (the adjacent sink nodes) will be added to the set of black circles (the aggregate nodes) is given by

$$p(k \in \circ \rightarrow k \in \bullet) = \frac{(a_k)}{\sum_{j \in \circ}(a_j)} \tag{15}$$

where a_k is the absorbed amount of tracer particles at position k. The growth process is modelled in this case by the addition of lattice sites in discrete space.

3.5.2. Accretive growth

The basic construction which is applied in the 3D geometrical model is shown in Fig. 7. The surface of the object is tessellated with a pattern of triangles, which are organized in a pattern consisting of mainly hexagons and pentagons. This pattern corresponds to the organization of the skeletal

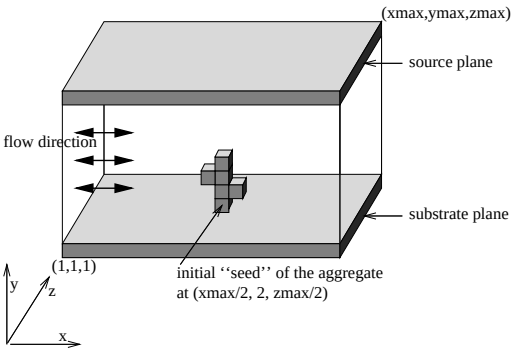

Figure 6: Basic construction of the aggregate.

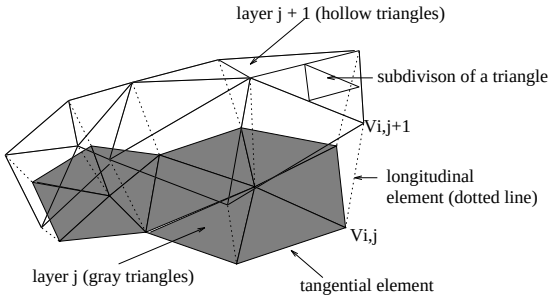

Figure 7: Construction of a new layer of triangles on top of the preceding layer. The triangles of the preceding layer are displayed in gray.

elements in the simulated organisms [14]. The edges of the triangles, the tangential elements, are of nearly equal size s, while the longitudinal elements vary between zero and s. In the construction the length l of a new longitudinal element, the edge connecting the vertices $V_{i,j}$ and $V_{i,j+1}$ of two successive layers, is determined by the growth function:

$$l = s \cdot k(c) \cdot h(\overline{r}, max\_curv) \qquad (16)$$

where $k(c)$ is an estimation of the local nutrient gradient and $h(\overline{r}, max\_curv)$ the amount of contact with the environment, a function based on the average local radius of curvature $\overline{r}$. This function models the capabilities of the transport system of the organism with which nutrients are transported through the tissue [14]. As soon as the amount of contact with the environment decreases and the amount of nutrients that can be transported is not sufficient, locally the growth velocity decreases. This function returns values below 1 as soon as a certain critical value, the maximum allowed radius of curvature *max_curv*, is exceeded.

In the construction the new longitudinal elements are set perpendicular with respect to the preceding tangential elements. The structure which emerges in this construction, a radiate accretive architecture, corresponds to the skeletal architecture found in the organisms with radiate accretive growth [14]. The construction starts with a sphere tessellated with triangles and in each step a new layer of tangential and longitudinal elements is constructed on top of the previous surface of the object. In Fig. 8 three successive stages in the growth process are shown. The tip-splitting in the object C is caused by the function $h(\overline{r}, max\_curv)$: as soon as the average local radius of curvature $\overline{r}$ exceeds the the maximum allowed value, locally the growth velocity decreases and the old branch splits into new branches.

One step in the iterative geometrical construction consists of 5 successive functional stages. Stage 1 is the actual geometrical construction as shown in Fig. 7. In stage 2 the amount of contact function $h(\overline{r}, max\_curv)$ is determined. In stage 3 triangles are respectively inserted or deleted in the new layer $j+1$. Insertion of triangles occurs if triangles become too large in the construction. In the simulation model the length of the tangential edge is only allowed to vary slightly around the basic unit s of the system. This unit corresponds to the size of the basic building elements (for example the size of spicules in sponges, corallites in stony-corals [14]) in the actual organisms. In for example Fig. 7 in layer $j+1$ in one of the triangles a critical limit is exceeded and the triangle is subdivided into four new ones. Also the reverse situation may occur, for example in triangles between branches the size of the edges may become smaller in subsequent growth steps. Triangles with edges below a certain critical lower limit are removed from the layer $j+1$. The insertion and deletion of triangles that are too large or too small ensures that in each iteration step a layer of almost equal-sized triangles is preserved and a pattern of triangles is mimicked which corresponds to the pattern found in real organisms [14]. Note that in the stages 1-3 the object is represented in continuous space.

In the next stage the geometrical object is mapped onto a 3D lattice with 144^3 sites. This discrete representation of the object next to the "normal" geometrical representation serves to approximate the nutrient distribution using the lattice Boltzmann method. In the nutrient distribution model the following assumptions are used: the nodes adjacent to the object nodes absorb tracer particles, resulting in a nutrient concentration zero at the sink nodes. A linear source of nutrient is introduced by releasing tracer particles at the top plane of the lattice. After the computation of the nutrient distribution the local nutrient gradients $k(c)$ are estimated in each site, along the normal vectors, on the surface of the object.

3.5.3. Parallelisation of the growth models

For the computation of the nutrient distribution using the lattice Boltzmann method combined with the tracer step, a parallel implementation was developed suitable for execution on a distributed memory machine. In the simulations a lattice consisting of 144^3 sites was used. In the parallel implementation this lattice was subdivided in the *xy*-plane into a number of sub-lattices, where each sub-lattice resides on a

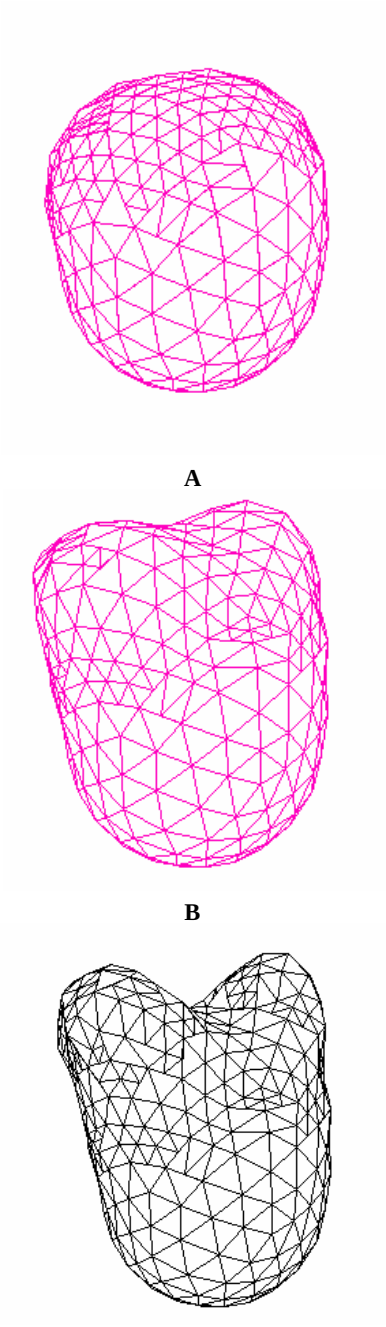

A

B

C

Figure 8: Three successive growth stages in the iterative geometrical construction

processor, and a where the complete lattice is mapped onto a virtual two dimensional torus topology of processors. The parallelized lattice Boltzmann solver, including the tracer step, was combined with both growth models.

In the aggregation model a complete parallized implementation was used, the algorithm described in pseudo-code consists of 4 stages:

```
                    :
1: initialisation of the aggregate, n_i's,
and tracer particles;
2: lattice Boltzmann iteration
  for n steps {
    update of n_i's sub-lattice;
    exchange n_i's between boundary planes
    sub-lattice;
  }
3: tracer step
  for n steps {
    release tracer particles at source
    nodes;
    move tracer particles over the sub-lattice;
    exchange tracer particles between
    boundary planes sub-lattice;
    absorb tracer particles at sink nodes;
  }
4: determine p (Eq. 15);
5: goto 2;
```

The nutrient distribution is computed in two parts: the lattice Boltzmann iteration in which the flow pattern around the aggregate is computed, and a tracer step in which the dispersion of particles due to diffusion and flow is determined. Both parts consists of a number of sweeps through the sub-lattice, after each sweep a local communication step is required in which the state of the boundary planes of the sub-lattices is updated by exchanging the states of boundary planes of neighbouring sub-lattices. In the growth step, in all possible growth candidates, the amount of absorbed tracer particles is determined, where a global communication step is required to determine the probability p (Eq. 15).

In the accretive growth model a hybrid implementation (see also [19]) was used in which a sequential implementation of stages 1-3 of the growth model is coupled with a parallel implementation consisting of the lattice Boltzmann solver and the determination of the local nutrient gradients. The hybrid implementation consisted of a sequential part, which runs on a normal workstation, and a parallel part which runs on a parallel computer. A description of the hybrid algorithm in pseudo-code is given below:

```
                :
0: a) initialisation of the geometrical
model (sequential part);
b) initialisation of the n_i's, and
tracer particles (parallel part);
1: construction of a new layer
(see Fig. 7) (sequential part);
2: estimation local radius of curvature
(sequential part);
3: insertion and deletion of triangles in
geometrical model (sequential part);
4: decomposition of the geometrical
model (sequential part);
5: communication between sequential and
parallel part;
mapping of the geometrical model onto
the sub-lattices (parallel part);
6: lattice Boltzmann iteration
(parallel part);
  for n steps {
    update of n_i's sub-lattice;
    exchange n_i's between boundary
    planes sub-lattice;
  }
7: tracer step (parallel part)
  for n steps {
    release tracer particles at source nodes;
    move tracer particles over the
    sub-lattice;
    exchange tracer particles between
    boundary planes sub-lattice;
    absorb tracer particles at sink
    nodes;
  }
8: estimation local nutrient gradients
(parallel part);
9: communication between parallel and
sequential part;
composition of local nutrient
gradients (sequential part);
10: goto 1;
```

In the hybrid algorithm the description of the geometrical object is commnunicated in step 5 from the sequential part to the parallel part. In the mapping of the geometrical model onto the sub-lattices in stage 5, the sink nodes around the object are specified, the object itself is represented a solid voxel object enclosed by the triangulated surface of the geometrical object. The results of the lattice Boltzmann iteration and tracer step, the local nutrient gradients, are communicated in step 9 from the parallel part to the sequential part.

In Fig. 9 a 3D aggregate is shown resulting from a simulation in which *Pe* was set to the value 0.0150. The aggregate in the figure is visualized by constructing a surface over the aggregate sites using the marching cubes method [22]. In Fig. 10 the nutrient distribution in a section made in the *xy*-plane, through the middle of the lattice, is shown. The colour shift black to white indicates a decrease in tracer particle concentration. The shape of the basins of equal nutrient ranges is displayed by colouring the adjacent basins black. The smooth shape of the basin is obtained by interpolating the results in the section with an original resolution of 144^2 data points. In Fig. 11 a similar section is shown through the nutrient distribution in an experiment in which *Pe* is set to the value 0.250. An example of an object obtained in 80 construction steps, and by setting *Pe* to the value 0.0150, of the accretive growth model is shown in Fig. 12.

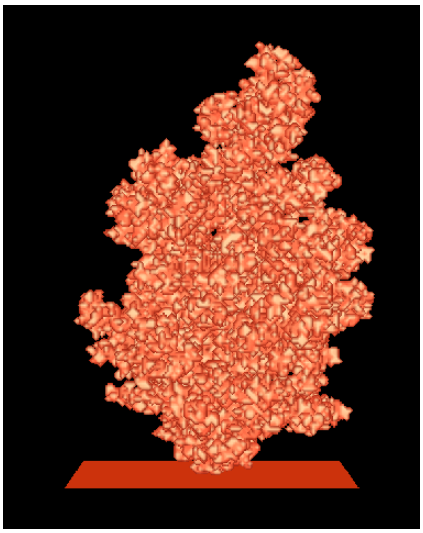

Figure 9: Aggregate resulting from a simulation where *Pe* is set to the value 0.0150 (the diffusion limited case).

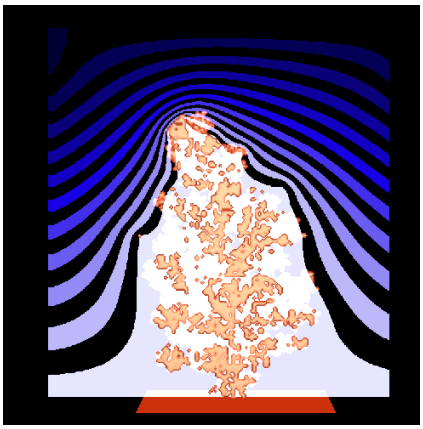

Figure 10: Nutrient distribution around an Aggregate where *Pe* is set to the value 0.0150 (the diffusion limited case).

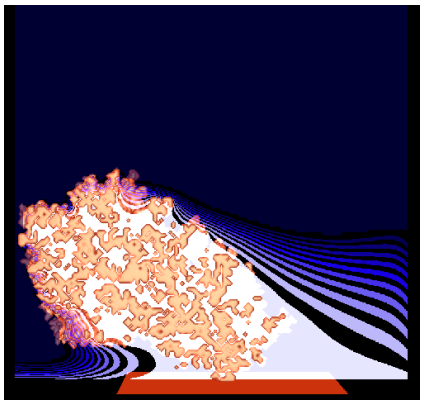

Figure 11: Nutrient distribution around an Aggregate where *Pe* is set to the value 0.250.

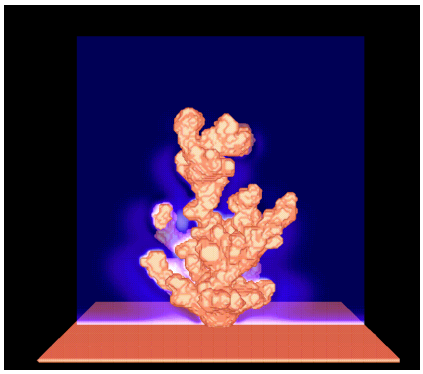

Figure 12: Object generated with the accretive growth model in 80 growth steps and where *Pe* is set to the value 3.0.

3.6. A comparison between the simulated and the actual marine sessile organisms

The lattice Boltzmann solver can be used to simulate the nutrient distribution in both the aggregative and accretive growth processes. In Figs. 10 and 11 it is demonstrated that the influence of hydrodynamics on the nutrient distribution occurs at higher *Pe* numbers. In the case of a low *Pe* number the diffusion limited sitation is obtained: an irregular object that is branching towards the nutrient source. At a higher *Pe* number the influence of the flow becomes visible: the object start to develop branches in the opposite direction of the flow, in the stream shadow of the aggregate an area depleted from nutrients occurs.

In the example of Fig. 12 it is demonstrated that is possible to model flow and diffusion limited growth by modelling the nutrient distribution with the lattice Boltzmann solver. In [19] we have discussed a 3D model for diffusion limited accretive growth in which the nutrient distribution was approximated with a "classical" method, by solving the diffusion equation with finite-differencing and Successive Over Relaxation. In the new version we have obtained a more general model which is capable of simulating diffusion and flow limited accretive growth. In the aggregates it is assumed that all nutrients are absorbed in the boundary nodes adjacent to the object, in many filter-feeding organisms there is a particle capturing mechanism present which allows the organism to utilize nutrients located at some distance from the organism. We are planning to include this aspect in our growth models.

We expect that models of diffusion and flow limited growth have a wide range of possible applications in biology and physics. Similar types of models may be applied to simulate growth of solid tumors and the dispersion of anticancer agents in vertebrate tissue (see [12]). Another important issue is the validation of growth models in which the effect of flow and diffusion is included. One option is to compare the simulated form to actual 3D growth forms using methods from mathematical morphology (see for example [15]). The other option is to carry out field or laboratory experiments in which the predictive value of the simulation model is tested, for example by testing if the effect of a change in the physical environment on the growth form can be predicted with the simulation model In for example [17] this was done by comparing the predictions of a two-dimensional growth model of a sponge to the actual results of transplantion experiments.

3.7. Diffusive patterning mechanisms

In many biological systems the distribution of chemical agents and nutrients, caused by a combination of flow and diffusion, plays a fundamental role. An example is morphogenesis where the external distribution of nutrients, as well as the internal distribution of morphogens in the organism, can induce certain growth patterns.

Reaction diffusion is one of the oldest mathematical models used for modelling biological pattern formation [33]. This model describes diffusing chemicals, where often a system of two antagonistic chemicals is used consisting of an activator and an inhibitor. This model can be described as a system of equations in the form [25]:

$$\begin{aligned} \frac{\partial A}{\partial t} &= F(A,I) + \mathcal{D}_A \nabla^2 A \\ \frac{\partial I}{\partial t} &= G(A,I) + \mathcal{D}_I \nabla^2 I \end{aligned} \tag{17}$$

In these equations A and I represent respectively the concentrations of the activator and the inhibitor. The functions F and G represent the reaction kinetics and the right terms in both equations the diffusion process, where $\mathcal{D}_A$ and $\mathcal{D}_I$ are the diffusion coefficients for the activator and inhibitor. The diffusion process can result in a heterogeneous spatial prepattern of chemical concentration distributions, in the case $\mathcal{D}_I$ is much larger than $\mathcal{D}_A$. In Turing's proposal for a

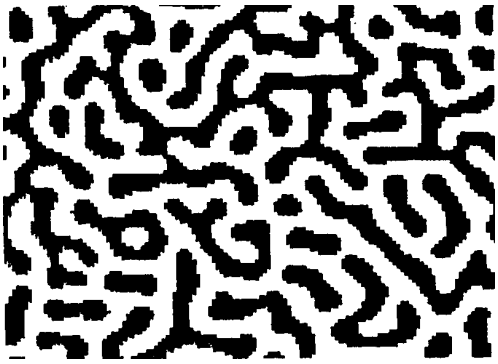

Figure 13: Simulation of a prepattern caused by diffusing activators and inhibitors in a 2D lattice. The cells in the lattice can be in two states: activated (black) or inhibited (white) (after [4]).

theory of morphogenesis, patterns or structures result from this prepattern. This prepattern can be defined as a heterogeneous spatial pattern of inhibitor and activator concentrations, while the resulting pattern can be considered as the realization of the prepattern. This model is especially suitable for generating patterns that may result more or less directly from this prepattern. It has been applied for simulating patterns found on shells, beautiful examples of this can found in [24]. An example of a simulation of such a prepattern is shown in Fig. 13. The diffusing activators and inhibitors are simulated on a 2D lattice, where the cells in the lattice can be in two states: activated (black) or inhibited (white) [3].

One of the most spectacular findings, this last decade, in biology is the discovery of the hox genes [8], [26], [29], [13]. which control the embryogenesis in animals (metazoans). The hox genes are the physical carriers of the genetic program which regulates embryogenesis. In for example *Drosophila* hox genes produce gradients of diffusing morphogens within the developing embryo which determine the body axes. In a cascade of activations of different genes, first the anterior-posterior axis, after this the dorso-ventral axis, and after this the segments are determined in the embryo. The gradients of diffusing morphogens provide the positional information required during the development of the embryo, although prepatterns are produced in the form of gradients, there is basically no activator inhibitor system required as in the reaction diffusion sytem of Eq. 17, but a cascade of gene activation. The remarkable thing about the hox genes is that these genes show a similar function in shaping the embryo across the animal kingdom. For example the gene *distalless* shapes the appendages in various metazoan phyla. Corresponding hox genes are active in the formation of body axes and in the construction of the body plan in distinctive metazoan phyla. The increase in complexity of the body plans in a range of phyla, as for example porifera (the sponges), cnidarians (for example stony corals), platyhelminthes, arthropods, and chordates. The complexity of the regulation of the growth process seems to be the lowest in sponges and the cnidarians (for example stony corals), which makes these organisms a very suitable case study for developing simulation models of growth and form in which both the influence of the physical environment and the biological regulation mechanism are included.

Acknowledgements

Jaap Kaandorp is very grateful to Benno Overeinder (Section Computational Science, University of Amsterdam), for his assistance and advice during the preparation of the manuscript. Jean Pierre Boon (Univerité Libre de Bruxelles, Belgium), kindly permitted me to use the picture in Fig. 13

References

1. E. Ben-Jacob. From snowflake formation to growth of bacteria colonies i: diffusive patterning in azoic systems. *Contemporary Physics*, 34:247–273, 1993. 1
2. E. Ben-Jacob. From snowflake formation to growth of bacteria colonies ii: cooperative formation of complex colonial patterns. *Contemporary Physics*, 38:205–241, 1997. 1
3. J.P. Boon, D. Dab, R. Kapral, and A. Lawniczak. Lattice gas automata for reactive systems. *Phys. Rep.*, 273:55–147, 1996. 11
4. J.P. Boon and A. Noullez. Development, growth, and form in living systems. In H.E. Stanley and N. Ostrowsky, editors, *On growth and form*, pages 174–183, Boston, 1987. Martinus Nijhoff. 11
5. J.C. Bythell. A total nitrogen and carbon budget for the elkhorn coral *acropora palmata* (Lamarck). *Proceedings of the 6th International Coral Reef Symposium*, 2:535–540, 1988. 4
6. S. Chen, Z. Wang, X. Shan, and G. Doolen. Lattice Boltzmann computational fluid dynamics in three dimensions. *Journal of Statistical Physics*, 68(3/4):379–400, 1992. 5
7. B. Chopard and M. Droz. *Cellular automata modeling of physical systems*. Cambridge Univerity Press, Cambridge, 1998. 5
8. D. Erwin, J. Valentine, and D. Jablonski. The origin of animal body plans. *American Scientist*, 85:126–137, 1997. 11
9. J. Feder. *Fractals*. Plenum Press, New York, London, 1988. 1, 2
10. H. Fujikawa and M. Matsushita. Bacterial fractal growth in the concentration field of nutrient. *J. Phys. Soc. Japan*, 60(1):88–94, 1991. 1, 3, 5

11. R.R. Graus and I.G. Macintyre. Variation in growth forms of the reef coral *montastrea annularis* (Ellis and Solander): a quantitative evaluation of growth response to light distribution using computer simulation. *Smithson. Contr. Mar. Sci.*, 12:441–464, 1982. 4

12. R.K. Jain. Barriers to drug delivery in solid tumors. *Scientific American*, July:42–49, 1994. 10

13. D. St Johnston and C. Nüsslein-Volhard. The origin of pattern and polarity in the *drosophila* embryo. *Cell*, 68:201–209, 1992. 11

14. J.A. Kaandorp. *Fractal modelling: growth and form in biology*. Springer-Verlag, Berlin, New York, 1994. 4, 5, 7

15. J.A. Kaandorp. Analysis and synthesis of radiate accretive growth in three dimensions. *J. Theor. Biol.*, 175:39–55, 1995. 10

16. J.A. Kaandorp. Morphological analysis of growth forms of branching marine sessile organisms along environmental gradients. *Mar. Biol.*, 134:295–306, 1999. 4

17. J.A. Kaandorp and M.J. de Kluijver. Verification of fractal growth models of the sponge *haliclona oculata* (Porifera; class Demospongiae) with transplantation experiments. *Mar. Biol.*, 113:133–143, 1992. 10

18. J.A. Kaandorp, C. Lowe, D. Frenkel, and P.M.A. Sloot. The effect of nutrient diffusion and flow on coral morphology. *Phys. Rev. Lett.*, 77(11):2328–2331, 1996. 5

19. J.A. Kaandorp and P.M.A. Sloot. Parallel simulation of accretive growth in 3-dimensions. *BioSystems*, 44(3):181–192, 1997. 5, 8, 10

20. A.J.C. Ladd. Numerical simulations of particulate suspensions via a discretized Boltzmann equation Part I. theoretical foundation. *J. Fluid Mech.*, 271:285–309, 1994. 5, 6

21. A.J.C. Ladd. Numerical simulations of particulate suspensions via a discretized Boltzmann equation Part II. numerical results. *J. Fluid Mech.*, 271:311–339, 1994. 5

22. W.E. Lorensen and H.E. Cline. Marching cubes: a high resolution 3D surface construction algorithm. *ACM Computer Graphics*, 21(4):163–169, 1987. 9

23. P. Meakin. A new model for biological pattern formation. *J. Theor. Biol.*, 118:101–113, 1986. 3

24. H. Meinhardt. *The algorithmic beauty of sea shells*. Springer-Verlag, Berlin, New York, 1998. Second Enlarged Edition. 11

25. J.D. Murray. *Mathematical Biology*. Springer-Verlag, Berlin, Heidelberg, 1990. 10

26. Pennisi and Roush. Developing a new view of evolution. *Science*, 277:34–37, 1997. 11

27. W.H. Press, B.P. Flannery, S.A. Teukolsky, and W.T. Vetterling. *Numerical recipes in C*. Cambridge University Press, Cambridge, 1988. 3

28. G. Punzo, F. Massaioli, and S. Succi. High-resolution lattice Boltzmann computing on the IBM SP1 scalable parallel computer. *Computers in Physics*, 8(6):705–711, 1994. 5

29. R.A. Raff. *The shape of life: genes, development, and the evolution of animal form*. The University of Chicago Press, Chicago, 1996. 11

30. D. H. Rothman and S Zaleski. *Lattice-Gas Cellular Automata*, volume 5 of *Collection Aléa-Saclay*. Cambridge University Press, Cambridge, UK, 1997. 5

31. L.M. Sander. Fractal growth processes. *Nature*, 322:789–793, 1986. 1, 2

32. L.M. Sander. Fractal growth. *Scientific American*, 256(1):82–88, 1987. 1

33. A.M. Turing. The chemical basis of morphogenesis. *Phil. Trans. Roy. Soc. Lond.*, B237:37–72, 1952. 10

34. J.E.N. Veron and M. Pichon. *Australian Institute of Marine Science Monograph series vol 1, Scleractinia of eastern Australia part 1*. Australian Government Publishing Service, Canberra, 1976. 4

35. F. Wiedenmayer. *Shallow-water sponges of the western Bahamas*. Birkhäuser, Basel, 1977. 4

36. C.R. Wilkinson, A.C. Cheshire, D.W. Klumpp, and A.D. McKinnon. Nutritional spectrum of animals with photosynthetic symbionts-corals and sponges. *Proceedings of the 6th International Coral Reef Symposium*, 3:27–30, 1988. 4

37. T.A. Witten and L.M. Sander. Diffusion-limited aggregation, a kinetic critical phenomenon. *Phys. Rev. Lett.*, 47(19):1400–1403, 1981. 6